Spin-up and the effects of a submarine canyon: Applications to upwelling in Astoria Canyon

R. Mirshak[1] and S. E. Allen

Department of Earth and Ocean Sciences, University of British Columbia, Vancouver, British Columbia, Canada

Received 6 July 2004; revised 17 October 2004; accepted 27 December 2004; published 17 February 2005.

[1] A parameterization for the on-shelf mass flux induced by upwelling through a shelf break submarine canyon is estimated by laboratory spin-up experiments. We determine the effects of a submarine canyon on flow evolution implicitly by measuring the topographic drag force in the context of a heuristic model. Trials were performed across a range of values for the shelf break velocity, Coriolis frequency, and buoyancy frequency. Assuming the drag force within the canyon is balanced locally by rotation, we propose a parameterization for upwelling through a canyon provided that the Coriolis frequency, buoyancy frequency, shelf break velocity, and canyon dimensions at the shelf break depth are known. We use our results to compare wind-forced and canyon-forced upwelling over Astoria Canyon off the coast of Washington State. The analysis suggests that canyon-forced upwelling through Astoria Canyon is of equal importance to wind-forced upwelling directly above it on seasonal scales.

Citation: Mirshak, R., and S. E. Allen (2005), Spin-up and the effects of a submarine canyon: Applications to upwelling in Astoria Canyon, *J. Geophys. Res.*, *110*, C02013, doi:10.1029/2004JC002578.

1. Introduction

[2] Shelf break submarine canyons are common bathymetric features that cut into the continental slope, extending past the shelf break and incising the continental shelf. They have horizontal length scales of about 10 km, and topographic slopes of up to 45°. When upwelling-favorable winds generate geostrophic shelf currents, upwelling is enhanced by the presence of submarine canyons [*Hickey*, 1997; *Allen et al.*, 2001]. The upwelled water can be from considerable depth: chemical signatures of upwelled water from Juan de Fuca canyon suggest a source of 400 m [*Freeland and Denman*, 1982], although the geometry of this canyon makes it a special case [*Allen*, 2000]; depths of about 300 m are more common [*Hickey*, 1997]. Field studies have examined the importance of canyon forced upwelling onto the continental shelf during isolated upwelling events [*Kinsella et al.*, 1987; *Hickey*, 1997; *Signorini et al.*, 1997], and have found that during a strong upwelling event, the cross–shelf break flux through a submarine canyon is an order of magnitude larger than what would be expected purely from wind-forced upwelling over a similar width of shelf break.

[3] Individual upwelling events last for several days, containing an early transient phase and a longer lasting, steady, advection phase. The transient phase is well described by linear dynamics [*Allen*, 1996] but due to the strength of nonlinear dynamics in the advection phase, its analytical description remains elusive. A present-day conceptual model of advection-driven flow through a canyon requires a geostrophically balanced shelf break current traveling in the direction opposite to Kelvin wave propagation (i.e., with the coast on the left if in the Northern Hemisphere). In a stratified system, the near-surface currents are not affected by the canyon but deeper currents are altered by it. Most flow across the slope continues past the canyon [*Klinck*, 1996], but some will turn into it. Once inside, the geostrophic currents are blocked by canyon walls, producing an unbalanced cross-shelf pressure gradient that drives flow up canyon [*Freeland and Denman*, 1982]. Furthermore, as water at shelf break depth flows over the canyon rim, it descends into the canyon. This descent results in vortex tube stretching [*Klinck*, 1996; *Hickey*, 1997], which results in the addition of cyclonic vorticity and turns the flow up canyon. Vorticity generated at the canyon walls during boundary layer separation can also be advected into the canyon [*Pérenne et al.*, 2001b]. Some of the water that is driven up canyon by vorticity and pressure gradients will be upwelled onto the continental shelf. It is our desire in this paper to examine this quantity of upwelled water. Deeper in the canyon, the currents steered up canyon cause the isopycnals to tilt, balancing the barotropic pressure gradient [*Allen*, 1996]. A more complete picture of flow through a canyon during upwelling favorable conditions is provided by *Allen et al.* [2001], and is summarized in Figure 2 of their paper. The flow field deeper in the canyon is also discussed by *Pérenne et al.* [2001a, 2001b].

[4] Numerical models have been used to describe the general nature of canyon flow [*Klinck*, 1996; *She and Klinck*, 2000] and have aided in the interpretation of field data, but due to steep canyon sides and strong vertical advection, truncation errors lead to numerical difficulties in replicating the flow field [*Allen et al.*, 2003]. Owing to the complexity of the flow field and relative paucity of field

[1]Now at Department of Oceanography, Dalhousie University, Halifax, Nova Scotia, Canada.

0148-0227/05/2004JC002578$09.00

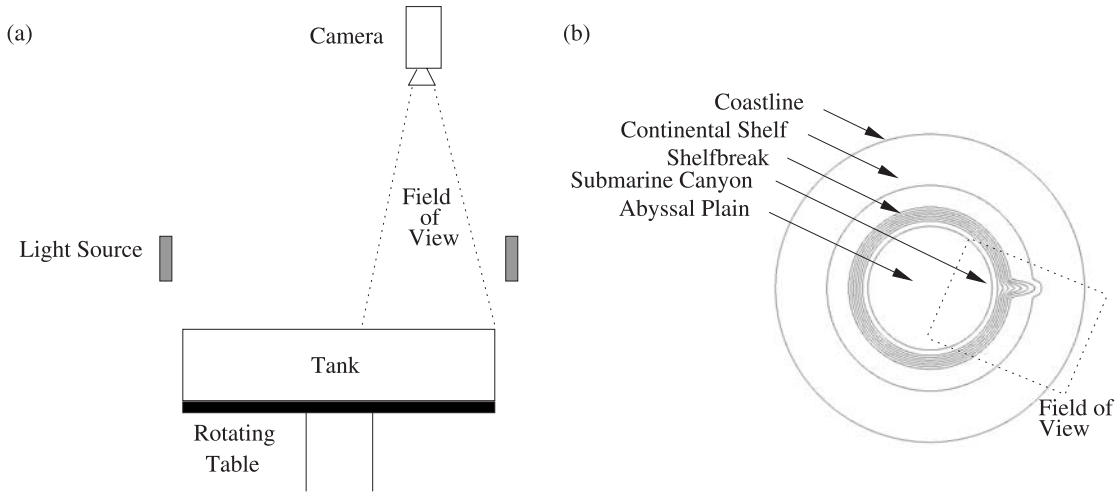

Figure 1. (a) Cartoon of the laboratory apparatus showing the cylindrical tank sitting on the rotating table. The light sources (fluorescent lights) and video camera are mounted in the rotating reference frame. (b) Plan view of the tank bathymetry. Contours show depth and are about 1 cm apart (Figure 2 has precise bathymetry). Laboratory experiments performed without a canyon present had radially symmetric topography. The field of view shown is approximate and varied slightly for different experiments.

data, numerical models are often tested against laboratory results [*Pérenne et al.*, 2001a, 2001b; *Allen et al.*, 2003; *Boyer et al.*, 2004] rather than oceanographic data sets. Observational studies have focused on strong and discrete upwelling events. Little has been done to examine how the upwelling flux in a canyon is affected by weaker currents, or if this flux is important over an extended period of time.

[5] Our study indirectly examined the upwelling flux in laboratory experiments by exploiting some unique attributes of the laboratory environment. By building a heuristic model that successfully describes spin-up in the absence of a canyon, we were able to infer the effect of a canyon on laboratory spin-up. (For a general review on this topic, see *Benton and Clark* [1974].)

[6] Differences in flow evolution without a canyon present in the laboratory (no canyon case) and with a canyon present (canyon case) allow us to infer the upwelling flux through the submarine canyon in the laboratory. The laboratory model is scaled such that its nondimensional parameters match those of Astoria Canyon, which cuts into the continental shelf of Washington State. We use laboratory results and hydrographic data to compare wind-forced and canyon-forced upwelling regimes over Astoria Canyon.

[7] The laboratory setup is described in section 2. In section 3, a heuristic model of laboratory spin-up in the absence of a canyon is presented. A comparison of the heuristic model to laboratory results is presented in section 4, showing the agreement in the absence of a canyon. The underprediction of spin-up with a canyon present is also shown. Section 5 uses the spin-up results to infer canyon-induced upwelling, which is then applied to Astoria canyon. Findings are summarized in section 6.

2. Methods

2.1. Laboratory Methods

[8] The tank used for these experiments is 1 m in diameter and the topography within mimics that of a generic coastal ocean: an abyssal plain in the tank center adjoins the continental slope, leading to a continental shelf and ending in a coastline at the tank edge. Calculations [*Allen et al.*, 2003; S. Jaramillo, personal communication, 2004] confirm that stratified flow passing through the canyon is hydrostatic. Hence so long as the Burger number is matched, the laboratory flow and ocean flow should behave in the same manner. In order to match the Burger number to oceanic conditions, vertical scales in the laboratory were exaggerated by an order of magnitude. To study the effects of a submarine canyon, a 22° slice of the continental slope was removed and replaced by a topographic section that mimics the bathymetry of a submarine canyon (Figures 1 and 2). For some experiments, the topography was radially symmetric (Figure 3), that is there was no canyon present in the bathymetry.

[9] In order to replicate flow through the canyon, the appropriate nondimensional parameters are identified and scaled in the laboratory (Table 1). We chose to scale the following four nondimensional parameters, using the length scales shown in Figure 4: (1) the Ekman number, $Ek = \delta/H_s$, where δ is the depth of the Ekman layer and H_s is the shelf break depth; (2) the Rossby number, $Ro = U/(f\mathcal{R})$, where U is the shelf break velocity, $f = 2\Omega$ is the Coriolis frequency where Ω is the rotation rate of the tank, and $\mathcal{R}$ is the radius of curvature of the upstream flank of the canyon; (3) the canyon Burger number, $S_c = (NH_s)/(fL)$, where L is the length of the canyon from its head to its mouth, $N = \sqrt{-(g/\rho_o)\partial\rho/\partial z}$ is the buoyancy frequency where g is gravity, ρ_o is a reference density, ρ is the density, and z is the vertical coordinate; and (4) the Froude number, $Fr = U/(NH_s)$. In determining the Ekman layer depth, we assume an eddy viscosity for the ocean but use molecular viscosity for laboratory calculations.

[10] The laboratory scaling is matched to oceanographic conditions around Astoria Canyon (Table 1). Control values of $N = 2.2\ s^{-1}$ and $f = 0.52\ s^{-1}$ were chosen. To test the sensitivity of canyon flow to these values, laboratory trials

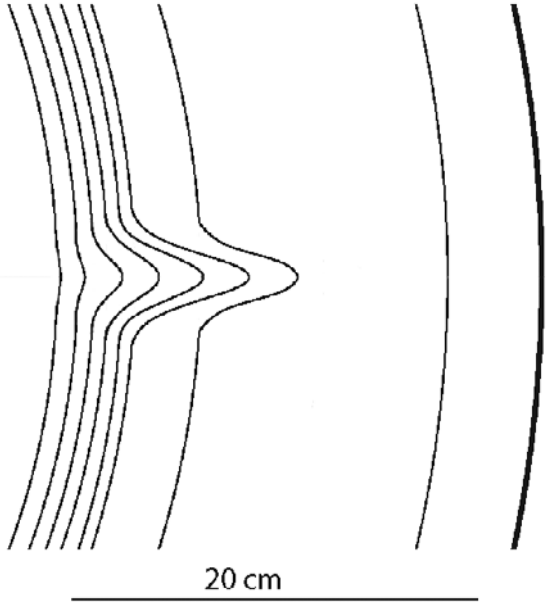

Figure 2. Canyon bathymetry used in laboratory experiments. The bold line represents the tank edge at r_e = 50 cm and is the coastline. The thin line closest to it is at 0.5 cm depth, and the bathymetry lines are 1 cm apart. The horizontal line across the bottom of the figure gives the scale.

were performed with individual parameters being changed separately (Table 2). Values for U were altered by changing the amplitude of forcing, and by changing the time of sampling within experiments. Hence having multiple results per trial allowed us to vary the velocity field within each trial, and we explored the effect of a canyon on spin-up across a region of S_c-Ro space (Figure 5).

[11] In an effort to minimize diapycnal mixing, the rotating tank was filled with stratified water over a period of approximately 90 min, and was left to spin-up for an additional 2 hours. Stratification was created using the *Oster* [1965] method with salt, so density diffusion is assumed negligible over the course of an experiment.

[12] Before forcing, the model in our laboratory consisted of a tank rotating at frequency Ω_o. Velocities were forced by imposing an angular acceleration on the tank. The acceleration persisted for one inertial period, after which the tank was rotating at $\Omega = \Omega_o + \Delta\Omega$. As a result, the velocity of the water in the tank (relative to the rotating tank) scales as the change in rotation rate, $\Delta\Omega$, multiplied by the tank radius r_e.

[13] Owing to the forcing methods used in our experiments, we produced a radially symmetric flow in geostrophic balance at first order. The forcing impulse was sufficiently long to allow development of an Ekman layer along the bottom, but short enough to leave the interior rotating at an approximately constant angular velocity, $-\Delta\Omega$. Hence the influences of rotation and advection on laboratory flow over a sloping bottom are described by the temporal Rossby number $Ro_t = \Delta\Omega/(f \cos\theta)$, where θ is the inclination from horizontal of the sloping bottom [*Pedlosky*, 1987]. In our experiments Ro_t ranged from 0.05 to 0.15 over the shelf and 0.09 to 0.26 over the slope.

2.2. Velocity Measurements

[14] Pliolite VT-L particles (provided by Goodyear) were used as surface tracers. In order to reduce surface tension, the water was treated with small amounts of surfactant. Surface velocities were realized by particle image velocimetry (PIV) methods [*Sveen*, 2000]. PIV examines the spectral characteristics of successive images to determine mean translation in pixels of a group of particles within an interrogation window. Error estimates based on the numerical experiments performed by *Raffel et al.* [1998] gave maximum velocity uncertainties dominated by displacement gradient error of about 5.6 mm s^{-1} on the continental slope and 3.5 mm s^{-1} over the continental shelf.

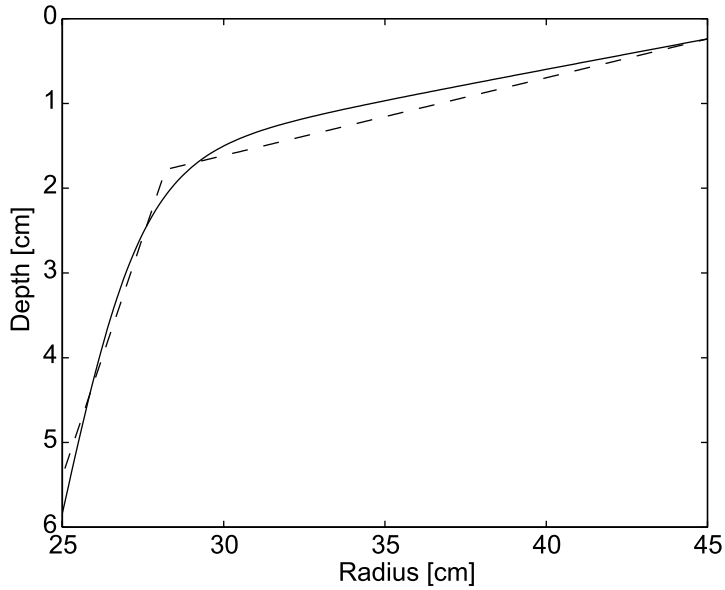

Figure 3. Section of radially symmetric topography (in the absence of a canyon) used in the laboratory (solid line) and topography used in the heuristic model (dashed line).

Table 1. Scaling of Parameters Used in Laboratory Modeling

Parameter	Symbol	Astoria	Lab
Radius of coast	r_e	...	50 cm
Radius of shelf break	r_{sb}	...	28.2 cm
Continental slope steepness	...	4°	54°
Canyon length	L	22 km	8.0 cm
Canyon width at shelf break	W_{sb}	16 km	5.8 cm
Shelf break depth	H_s	150 m	2.0 cm
Maximum depth	H_d	750 m	10 cm
Radius of curvature into the canyon	$\mathcal{R}$	4.5 km	4.0 cm
Bottom Ekman layer depth	δ	50 m	2 mm
Buoyancy frequency	N	7.5×10^{-3} s^{-1}	2.2 s^{-1}
Coriolis frequency	f	10^{-4} s^{-1}	0.5 s^{-1}
Shelf break velocity	U	20 cm s^{-1}	1.2 cm s^{-1}
Ekman number	Ek	0.33	0.10
Canyon Burger number	S_c	0.51	1.1
Froude number	Fr	0.18	0.27
Rossby number	Ro	0.44	0.58
Temporal Rossby number	Ro_t	...	0.1
Fractional depth	H_s/H_d	0.2	0.2
Horizontal aspect ratio	W/L	0.73	0.725

[15] As radial symmetry is assumed, the initial condition for the spin-up model (described in the following section) was a fit to all data within the field of view window (see Figure 1) with the restriction that $r > 20$ cm. This boundary was chosen because spin-up behavior in the inner portion of the tank occurs over a much larger timescale than over the slope, so radial velocities in that region are approximately constant over the time of our experiments. In order to interpolate our velocity measurements onto a regular grid, the laboratory data were fit to a fourth-order polynomial that was forced to match a no-slip boundary condition at the tank edge, $r_e = 50$ cm:

$$v(r) = C_1(r - r_e) + C_2(r - r_e)^2 + C_3(r - r_e)^3 + C_4(r - r_e)^4,$$

which can also be written in matrix form as

$$\mathbf{v} = \mathbf{RC}. \tag{1}$$

[16] The value of the coefficient $\mathbf{C}$ was investigated by assuming that the measured laboratory velocities are close enough to the real values that their error bears a normal distribution [*Press et al.*, 1986, section 14.5]. A Monte Carlo method was then used where a random selection of 100 points was taken from the laboratory data (whose abundance ranged from 110 to 172 points depending on the run) and had a normally distributed error added to it. The coefficient was then found by matrix inversion. This process was iterated 100 times, with a coefficient matrix, $\mathbf{C}_i$, produced for each iteration:

$$\mathbf{C}_i = (\mathbf{R}'\mathbf{R})^{-1}\mathbf{R}'(\mathbf{v}_i + \mathbf{E}_i\delta\mathbf{v}_i), \tag{2}$$

where $\mathbf{v}_i$ represents the randomly selected laboratory data used to find the coefficients of the ith iteration, $\mathbf{E}_i$ is a normally distributed set of random numbers with a mean of zero and a variance of one, and $\delta\mathbf{v}_i$ is the uncertainty of the velocity values in $\mathbf{v}_i$, based on the results of *Raffel et al.* [1998] and the methods of *Press et al.* [1986]. The gridded velocity $\mathbf{V}$ was found by entering the values of $\mathbf{C}_i$ into (1):

$$\mathbf{V} = \frac{1}{100}\sum_{i=1}^{100}\mathbf{V}_i = \frac{1}{100}\sum_{i=1}^{100}\mathbf{RC}_i, \tag{3}$$

with the uncertainty in $\mathbf{V}(r)$ being twice the standard deviation of the $\mathbf{V}_i(r)$ values. Goodness of fit was examined by performing a chi-square test, and then evaluating Q, the probability that the actual chi-square exceeds the calculated value by chance [*Press et al.*, 1986, section 15.1]. We rejected runs for which $Q < 0.05$. The resulting fit and error estimates were used to set initial conditions for, and to compare lab results to, the heuristic spin-up model developed in the following section.

3. Spin-Up Model

3.1. Overview of the Spin-Up Process

[17] In the classic spin-up experiment [*Greenspan and Howard*, 1963], a cylindrical, rigid walled tank containing a viscous, homogeneous fluid in solid body rotation has its angular velocity increased by a small amount. Viscous stresses in the boundary layers create a centrifugal force that overwhelms the pressure gradient, causing a radially outward Ekman transport. This transport is balanced by a vertical transport from the interior, which undergoes vortex tube stretching. The stretching increases the angular velocity of the interior, causing it to achieve solid body rotation (hence spin-up) far quicker than by nonrotating, frictional physics.

[18] Stratification alters spin-up as buoyancy forces begin to play a role. Some important results are that the Taylor-Proudman constraint breaks down [*Hogg*, 1973]. In the absence of friction in the interior, the final spin-up state is nonuniform with rotation rates varying vertically in the fluid over the length scale $r_e f N^{-1}$ [*Holton*, 1965], where r_e is the tank radius. When the bottom boundary is sloped, buoyancy effects within the boundary layer must also be considered [*MacCready and Rhines*, 1991].

3.2. No Canyon Case

[19] In this section we provide a solution to the spin-up of fluid in a cylinder over radially symmetric, sloping topography, consistent with our laboratory setup in the absence of a canyon. A steady geostrophic flow traveling over a bottom will generate a bottom Ekman layer. Following conservation of mass arguments, horizontal shear in the interior results in Ekman pumping into/out of the bottom boundary layer [*Greenspan*, 1968]. If we consider a homogeneous fluid in a radially symmetric, geostrophic flow as it travels over a bottom that slopes at an angle θ, where θ is small, then the velocity out of the boundary layer is (following *Pedlosky* [1987])

$$w = \sqrt{\frac{\nu}{4f}}\zeta\cos\theta, \tag{4}$$

where ν is the kinematic viscosity of water, ζ is the vorticity of the radially symmetric flow and is defined as

$$\zeta = \frac{1}{r}\frac{\partial}{\partial r}(rv),$$

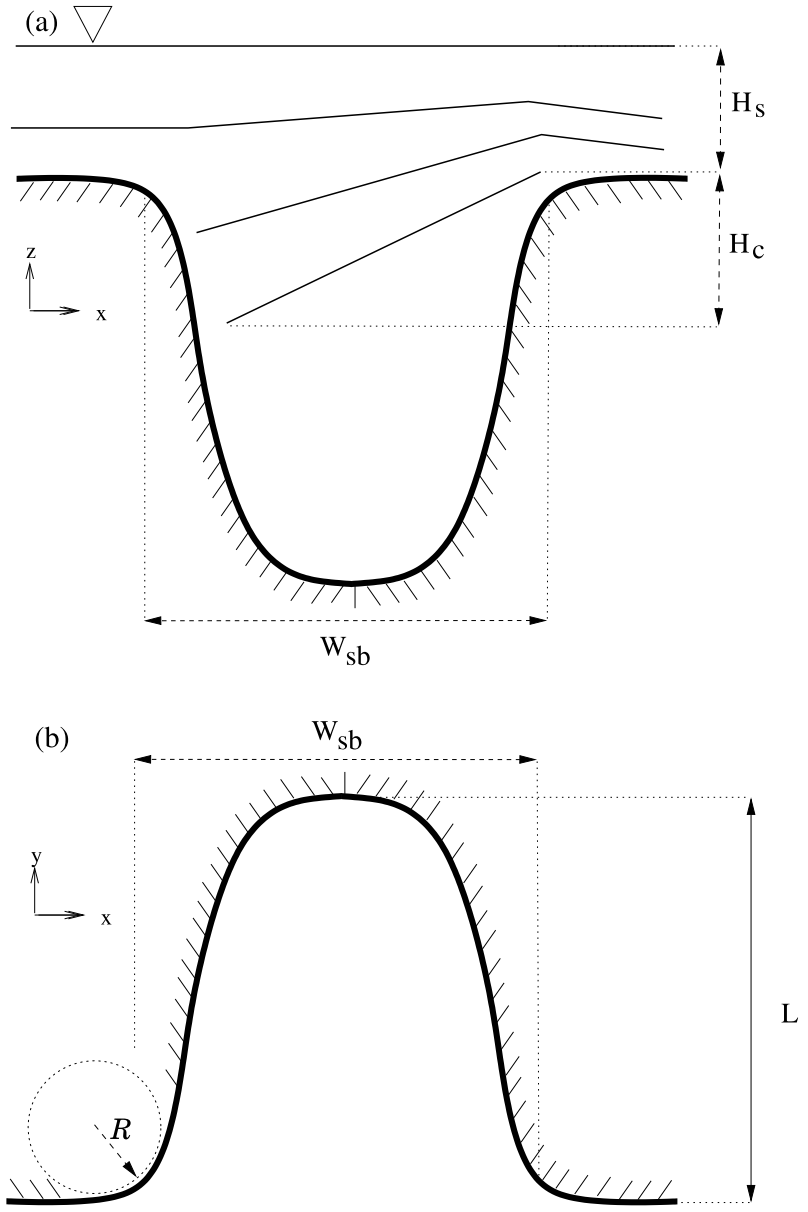

Figure 4. Length scales that need to be considered for this problem. For, upwelling-favorable conditions the currents over the shelf travel in the x direction. The bold line represents topography. (a) Cross section of the canyon at the shelf break. Thin lines represent isopycnal surfaces. (b) Plan view of the canyon. The topographic line is the isobath of the shelf break.

and v is the (assumed radially symmetric) azimuthal velocity. One effect of having a bottom slope is that the Rossby number for boundary layer flow over the slope increases as csc θ [e.g., *Pedlosky*, 1987]. Linear dynamics continue to describe Ekman suction, provided that the Rossby number is less than 0.5 [*Hart*, 2000]. This constraint is satisfied throughout our laboratory setup and the predictive success of a linear model is verified by laboratory results presented later in this paper.

[20] For our experiments, the vertical scale over which rotation rates change during spin-up of a stratified fluid is much greater than the water depth over the region of interest in our laboratory. As the water depth $h \ll (r_e f N^{-1})$, we assume that the spin-up of a stratified fluid due to Ekman

Table 2. Different Values of Stratification and Rotation Used in Laboratory Experiments[a]

Trial	N_{SB}, s^{-1}	f, s^{-1}
1	2.2	0.52
2	**4.4**	0.52
3	2.2	**0.40**
4	2.2	**0.70**

[a]Each trial was performed with and without a canyon present in the tank topography, with different values for the change in rotation rate, $\Delta\Omega$. Deviations from standard values are boldfaced.

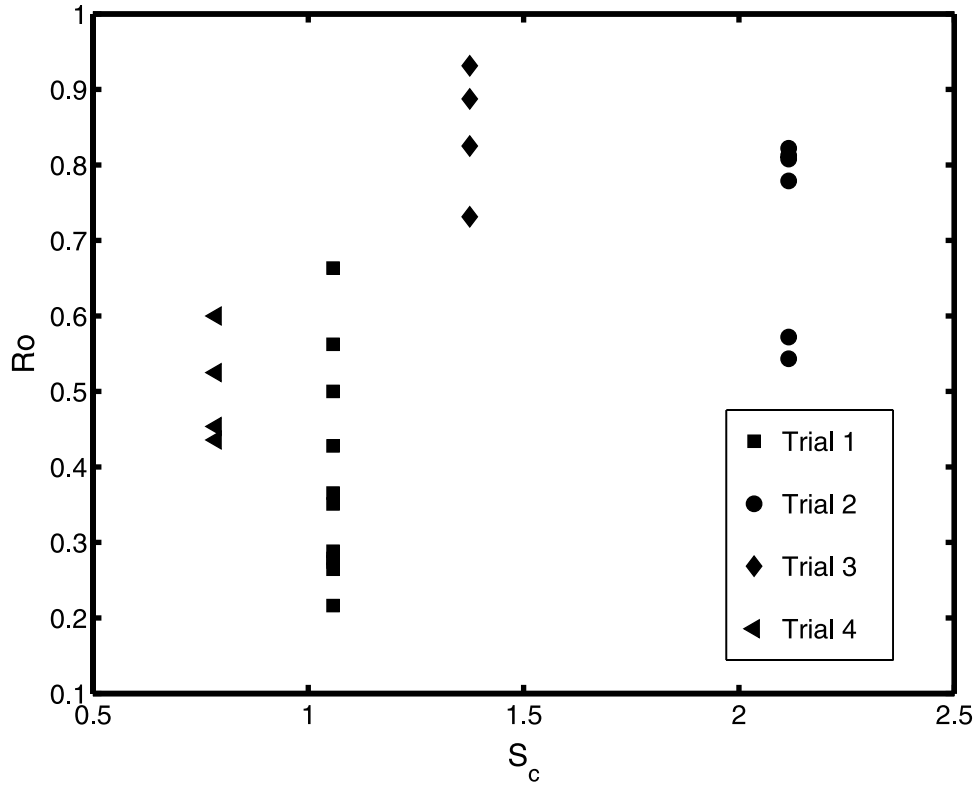

Figure 5. Locations in S_c-Ro space where spin-up with a canyon was examined in the laboratory. There were several runs performed for each of the four trials, which are summarized in Table 2.

suction is vertically homogeneous over the shelf/slope region of our experiments.

[21] If friction is negligible in the interior, the flow is axisymmetric, and Ro_t is small enough to ignore advective terms above the boundary layer, then taking the curl of the horizontal component of the equation of motion and employing the continuity equation gives

$$\frac{\partial}{\partial t}\left(\frac{f+\zeta}{h}\right) = 0. \tag{5}$$

If it is assumed that for a fluid particle in the interior, $\partial h/\partial t = -w$ where the interior meets the bottom Ekman layer, (5) can be written as a differential equation for ζ:

$$\frac{\partial \zeta}{\partial t} = -\frac{w}{h}(f+\zeta), \tag{6}$$

where w is given by (4). For our experiments, changes in $h(r)$ are of $O(h)$. Hence $\partial\zeta/\partial t$, which is dependent on h, varies considerably across the tank, as does the timescale for the evolution of ζ (the spin-up timescale).

[22] When stratification is introduced to the spin-up problem over a sloping bottom, the upslope transport in the Ekman layer redistributes the density field, advecting denser fluid into a region of less dense fluid. Buoyancy forces eventually become as large as Coriolis effects, effectively shutting down the boundary layer and insulating the interior from the bottom. In this limit there is no Ekman suction and the flow evolves as

$$\frac{\partial v}{\partial t} = \nu\left(\sin^2\theta + \frac{S_s}{1+S_s}\cos^2\theta\right)\frac{\partial^2 v}{\partial z^2} + \nu\left(\frac{S_s}{1+S_s}\sin^2\theta + \cos^2\theta\right)\nabla_H^2 v \tag{7}$$

(after *MacCready and Rhines* [1991]), where z is vertical (i.e., not normal to the slope), $\nabla_H^2 X = r^{-1}\partial(rX)/\partial r$ represents the radial components of the Laplacian operator on some variable, X, and $S_s = (N \sin\theta/f\cos\theta)^2$ is a slope Burger number. Horizontal diffusion is not included in the model of *MacCready and Rhines* [1991] but must be included here because depth changes near the shelf break are rapid enough that a horizontal shear develops in the flow. Boundary layer shutdown will occur on the timescale $\tau = S_s/[(1+S_s)S_s^2 f\cos\theta]$ [*MacCready and Rhines*, 1991].

[23] Laboratory results are well predicted by a heuristic model based on (6) and the work of *MacCready and Rhines* [1991]. For laboratory simulations, the shutdown timescale τ over the continental shelf ranged from 2 s ($f = 0.52$ s^{-1}, $N = 4.4$ s^{-1}) to 20 s ($f = 0.52$ s^{-1}, $N = 2.2$ s^{-1}). (For $f = 0.52$ s^{-1}, one inertial period is about 12 s.) The shutdown process is gradual and Ekman suction into the boundary layer (and therefore its influence on spin-up) will decay on the shutdown timescale. In our experiments, a change in the value of $\partial\zeta/\partial t$ over the shelf is observed to occur over the

shutdown timescale. Flux out of the boundary layer becomes a time-varying version of (4):

$$w = G\zeta\sqrt{\frac{\nu\cos^2\theta}{4f}}\left(\frac{\tau}{t}\right)^{1/2}, \tag{8}$$

where G is a constant and t is the time since spin-up began [*MacCready and Rhines*, 1991]. The $t^{-1/2}$ dependence is due to buoyancy effects inhibiting the upslope transport in the bottom Ekman layer, and is discussed by *MacCready and Rhines* [1991]. Equation (8) suggests that $w \sim \infty$ as $t \rightarrow 0$ and so the model cannot be used for small values of t/τ. *MacCready and Rhines* [1991, Figure 2] compares predicted mass flux in a sloping bottom Ekman layer from their theory to numerical simulations. They find $G = 0.8072$ converges upon their numerical predictions, especially after $t/\tau > 12$. For the continental shelf in the laboratory, we examine the regime at a time when t/τ is between 2 and 4. On the basis of the results presented in their Figure 2, for our regime G is close to 0.95. We assume $G = 1$.

[24] The shutdown timescale was derived for a small slope, where $\sin\theta \approx \theta$ [*MacCready and Rhines*, 1991]. For the continental slope region, $\theta \approx 56°$ and we are beyond this proposed domain. For our study, this steep slope does not affect model results. If the bottom Ekman layer does form and shut down, it will be on a timescale of $O(10^{-2}$ s). If the side wall is too steep for an Ekman layer to develop on the timescale of an experiment, the slope would act as a no-slip sidewall boundary. Given the topography in the laboratory, the *e*-folding time required for friction effects on the slope to be realized at the surface is 400 s at the shelf break, increasing rapidly with depth over the continental slope. The duration of our experiments (60 s) is therefore too small to observe any effects, as is verified by results presented in the next section.

[25] The diffusive behavior of the flow is modelled to vary on the shutdown timescale as well. Early in time, diffusion above the boundary layer is isotropic ($\nu\nabla^2 v$). By the end of boundary layer shutdown, however, the diffusion will follow the right hand side of (7). As such, it can be expected that the diffusion will change from isotropic diffusion to (7) over the shutdown timescale:

$$\left\{\left(\frac{\tau}{t}\right)^{1/2}\nabla^2 + \left[1-\left(\frac{\tau}{t}\right)^{1/2}\right]\left[\left(\sin^2\theta + \frac{S_s}{1+S_s}\cos^2\theta\right)\frac{\partial^2}{\partial z^2} + \left(\frac{S_s}{1+S_s}\sin^2\theta + \cos^2\theta\right)\nabla_H^2\right]\right\} v. \tag{9}$$

[26] Over the duration of the experiments, flow evolution in the tank changes from being controlled primarily by Ekman suction (6) to being controlled by the diffusion as described in (9). As such it is necessary to represent both effects. As the processes described here are linear, $\nabla \times$ (9) inserted into (6) gives an appropriate description of spin-up:

$$\left\{\frac{\partial}{\partial t} - \nu\left(\frac{\tau}{t}\right)^{1/2}\nabla^2 - \nu\left[1-\left(\frac{\tau}{t}\right)^{1/2}\right]\left[\left(\sin^2\theta + \frac{S_s}{1+S_s}\cos^2\theta\right)\frac{\partial^2}{\partial z^2} + \left(\frac{S_s}{1+S_s}\sin^2\theta + \cos^2\theta\right)\nabla_H^2\right]\right\}\zeta = -\frac{w(t)}{H}(f+\zeta), \tag{10}$$

where $w(t)$ is defined by (8). Equation (10) is hereafter referred to as our "heuristic model." It is solved numerically using a finite difference scheme over a slightly simplified topography (Figure 3), and its results are compared to those from laboratory experiments.

[27] The value of ζ was solved using forward Euler differentiation, $\partial/\partial r$ terms were solved with the leapfrog method, and second-order derivatives were solved with a centered second-order scheme. Integrations were determined using a forward Euler scheme. The value for v was determined from ζ using a no-slip boundary condition at the tank edge. Discretizations of $\Delta r = \Delta z = 0.25$ cm and $\Delta t = 0.0625$ s gave stable solutions. Experimentation with different discretizations suggested that the solution was not sensitive to the chosen values. The domain examined in our heuristic model extended from $r = 25$ cm to $r = 45$ cm, with a free-slip constraint at both edges. (The shelf break is located at $r_{sb} = 28$ cm, the tank edge is located at $r_e = 50$ cm.)

[28] Laboratory measurement methods, described in section 2.2, give 100 approximations of the velocity field at each time for each trial. To propagate uncertainty through the heuristic model, all these approximations were used as initial conditions, with the mean and standard deviations of the output velocity field being calculated.

[29] It is important to note that our laboratory model is designed to replicate flow patterns through the canyon. The spin-up behavior of the tank, and the timescales for boundary layer shutdown, do not scale to match oceanic flows nor are they meant to.

3.3. Canyon Case

[30] When a canyon is inserted into the topography, we anticipate an increase in the spin-up rate. As flow past a canyon evolves during the transient phase of upwelling, a train of standing waves develops downstream of the canyon. Similar waves do not form under downwelling conditions [*Durrieau de Madron*, 1994] and under oscillatory ocean flows, such as tides, these waves are thought to cause a rectified flow over the shelf. In laboratory studies, oscillatory flow over a canyon was found to impose a drag for barotropic [*Pérenne et al.*, 1997] and baroclinic [*Pérenne et al.*, 2001a] cases. Our experiments, however, do not impose oscillatory flow; due to the insulating nature of the shutdown Ekman layer in our experiments, however, we do not expect the wave drag effects to be large. Instead, for our laboratory model we infer a form drag within the canyon itself.

[31] The difference in spin-up due to the form drag can be likened to an impulse, and therefore an average force, applied on the water by the canyon over some time Δt. We infer the form drag to be

$$F_d = \frac{2\pi\rho}{\Delta t}\int_{r_{sb}}^{r_e}\Delta v(r)h(r)r\,dr, \tag{11}$$

where F_d is the average drag force applied over the time Δt, Δv is the difference between the velocity predicted by the heuristic model over the time Δt and that measured in the laboratory with a canyon present in the topography, r_{sb} is the location of the shelf break, h is the water depth and r is the radial coordinate. The form drag is caused by the

difference in pressure integrated over the upstream and downstream sides of the canyon. The combined effects of this drag with rotation allow us to infer canyon upwelling, which is described in the discussion.

[32] To find F_d, it is necessary to measure tank velocity from laboratory measurements at an initial time, use these measurements to predict spin-up by the heuristic model, and compare the heuristic model output after Δt to velocities measured in the laboratory after that same interval. Uncertainty in F_d is determined from the uncertainty of Δv, where we assume a normal error distribution for both the model output velocity and the measured laboratory velocity.

[33] In order to determine how the fluid and flow properties affect this drag, we introduce a parameterization for the drag, F_p:

$$F_p = \rho C_d \ell_1 \ell_2 U^2, \tag{12}$$

where C_d is a drag coefficient, ℓ_1 and ℓ_2 are length scales, and U is the velocity at the shelf break. The product of ℓ_1 and ℓ_2 give the effective area of the canyon projected on a plane normal to the flow U [*Batchelor*, 1967]. This parameterization essentially models a form drag, hence the length scales should be independent of bottom slope within the canyon. The slope angle of the canyon walls does not enter our model because the upwelled water travels along isopycnals that rise O(100 m) over O(10 km). Given that canyon slopes have an aspect ratio close to unity, boundary processes should not considerably affect the upwelling signal.

[34] For the length scales ℓ_1 and ℓ_2, we propose the length of the canyon, L, and the depth in the canyon from which water is advected onto the shelf, H_c (Figure 4). Waters in the canyon below H_c that recirculate within the canyon or exit the canyon below the shelf break are not of interest here and are believed to affect neither the predictions of upwelling that result in the laboratory nor the ability to extrapolate these results to Astoria Canyon.

[35] In order to relate H_c to quantities that can be directly measured (from a bathymetric chart, for instance), consideration of the upwelling current as it passes through the canyon is required. The large-scale upwelling flow that passes through a canyon is dependent on the vortex stretching associated with cross-isobath flow over the upstream flank of the canyon [*Hickey*, 1997], as well as the effects of the geostrophic pressure gradient [*Freeland and Denman*, 1982]. If $Ro \ll 1$, flow will essentially follow isobaths through the canyon and there will be no significant upwelling of deeper water. As Ro increases, the cross-isobath flow will increase, and waters traveling down into the canyon will undergo vortex tube stretching, which ultimately increases the upwelling strength [*Hickey*, 1997]. Hence $H_c \propto Ro^k$, where $k > 0$. The stronger the stratification, the greater the available potential energy that must be overcome by upwelling currents so we also have $H_c \propto S_c^{-1}$.

[36] The shelf break depth H_s is dynamically irrelevant to flow through the canyon but is a component used to find S_c. To remove it from the parameterization, we introduce a scale height $H_{sc} = H_s S_c^{-1} = LfN^{-1}$, giving $H_c \propto H_{sc} Ro^k$. This scale height, it turns out, is the vertical length scale to which a topographic feature of length L will affect flow in a rotating, stratified fluid [*Hogg*, 1973].

[37] Hence we fit the parameterization of the drag imposed by the canyon to

$$F_p = \rho C_d L^2 (f/N) Ro^k U^2. \tag{13}$$

U, Ro, and N, were measured and varied in the laboratory, canyon dimensions were constant in our experiments, and values for C_d and k were determined from laboratory results.

4. Results

4.1. No Canyon Case

[38] The heuristic model (10) describes the spin-up of a stratified fluid over a slope, and is used to predict laboratory spin-up when a canyon is not present, using the topography shown in Figure 3. This model was tested against a series of laboratory experiments with various values of N, f, and U. Velocities determined from the laboratory model were used as initial conditions for our heuristic model, and the laboratory results that followed later in time were compared to the predictions.

[39] Spin-up results for a homogeneous fluid show that the linear Ekman solution properly represents suction into the boundary layer over a steep slope (Figure 6). The model mildly over predicts the spin-up rate near the tank edge, but agrees with laboratory measurements over the shelf break region. This result indicates that the topography used for the heuristic model correctly predicts the effects of Ekman suction on spin-up across the shelf region of the laboratory experiments. An inertial wave is observed in the velocity field, most noticeably in Figures 6d, 6g, and 6i. These three figures are separated by approximately one inertial period, and in all cases, the velocity field is temporarily lower than predicted values.

[40] When stratification is introduced, the effects of boundary layer shutdown alter spin-up over the sloping bottom of the tank, slowing the spin-up process (Figure 7). There are examples in Figure 7 where the heuristic model temporarily over- or underpredicts the speeds measured in the laboratory. Unlike the homogeneous case, the inertial oscillations present in stratified trials cause a more considerable increases or decreases in speed. At times coincident with the inertial period, however, the spin-up model successfully replicates the spin-up process of the laboratory model. The spin-up rate is slower than for the homogeneous fluid, which is an indication of the boundary layer shutdown process. The agreement at the shelf break indicates that the assumptions made for the boundary over the steeply sloping bottom in section 3.2 do not affect our results.

4.2. Canyon Case

[41] In order to determine the effect of a submarine canyon on laboratory spin-up, experiments with a canyon present were tested against our heuristic spin-up model. Initial conditions were set in the same manner as for the no canyon case, but here a difference in flow evolution was present one rotation period of the tank later (Figure 8).

[42] We determine F_d by assuming that it is balanced purely by acceleration of the shelf flow in the laboratory, thereby decreasing the spin-up rate. Values of F_d, U, Ro, and N from the various trials were used to solve for C_d and k in (13). A regression in log-space finds $k = 0.66 \pm 0.35 \approx 2/3$.

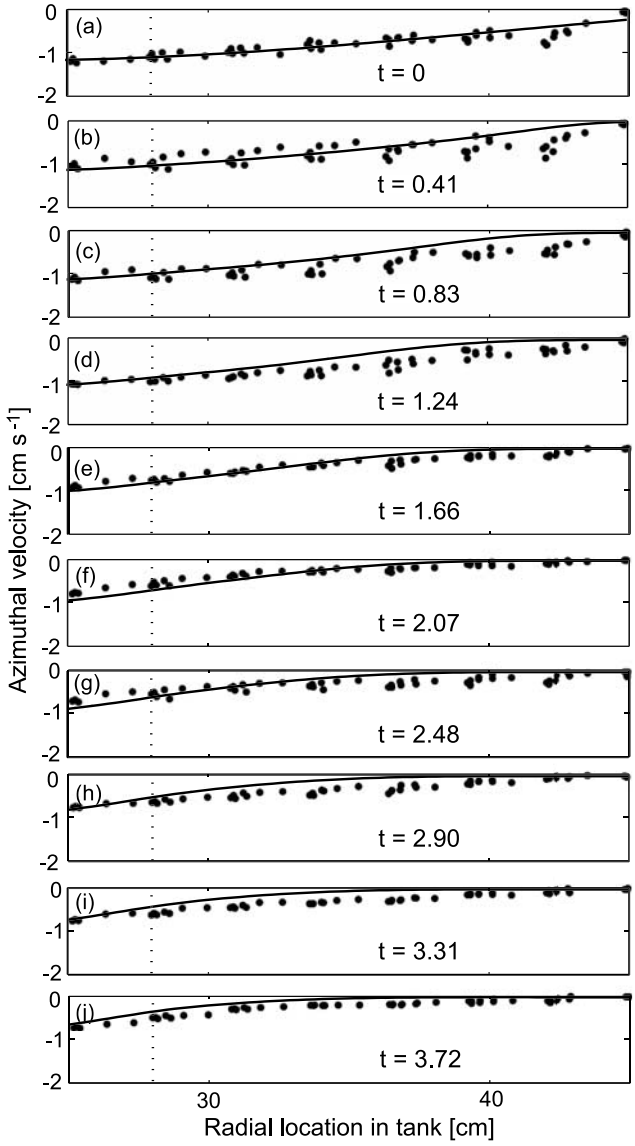

Figure 6. Comparison of laboratory spin-up measurements (dots) with heuristic model predictions (solid lines) for a homogeneous fluid and $f = 0.52\ s^{-1}$. The time shown in the panels is scaled by $2\pi f^{-1}$ and is nondimensional. Plots show azimuthal velocity over the laboratory continental shelf at (a) 0 s, (b) 5 s, (c) 10 s, (d) 15 s, (e) 20 s, (f) 25 s, (g) 30 s, (h) 35 s, (i) 40 s, and (j) 45 s. A fit to data at 0 s is used for the initial conditions. The dotted line represents the location of the shelf break (28.2 cm).

Using $k = 2/3$, C_d is found by linear regression to be $C_d = 0.43 \pm 0.02$, where the uncertainty represents the standard error (Figure 9). This parameterization gives an r^2 value of 0.95. The data used to produce Figure 9 are replicated in Table 3.

5. Discussion

[43] The use of our drag force parameterization is now used to infer upwelling through a canyon. The drag generated cannot be balanced by acceleration within the canyon itself. This would lead to waters within the canyon achieving solid body rotation before the waters on the shelf, but there is continuous flow through the canyon during the spin-up process [*Pérenne et al.*, 2001b; *Allen et al.*, 2003]. For velocities equal to $U_c = O(10^{-2}\ m\ s^{-1})$ in the laboratory canyon and $U_c = O(10^{-1}\ m\ s^{-1})$ in the an ocean canyon, the values in Table 1 give $U_c/(fL) \approx 0.25$ and 0.05 for the laboratory and ocean, respectively. Assuming that flow through the canyon is geostrophic implies its strength is directly related a cross-canyon pressure gradient ($fv = (1/\rho)\partial p/\partial x$). Recalling that the pressure difference across the canyon is directly related to the form drag links the flow through the canyon to the form drag.

[44] Under the assumption of geostrophic balance of the drag in the canyon we find that

$$fv_{up} = \frac{F_p}{V\rho}, \tag{14}$$

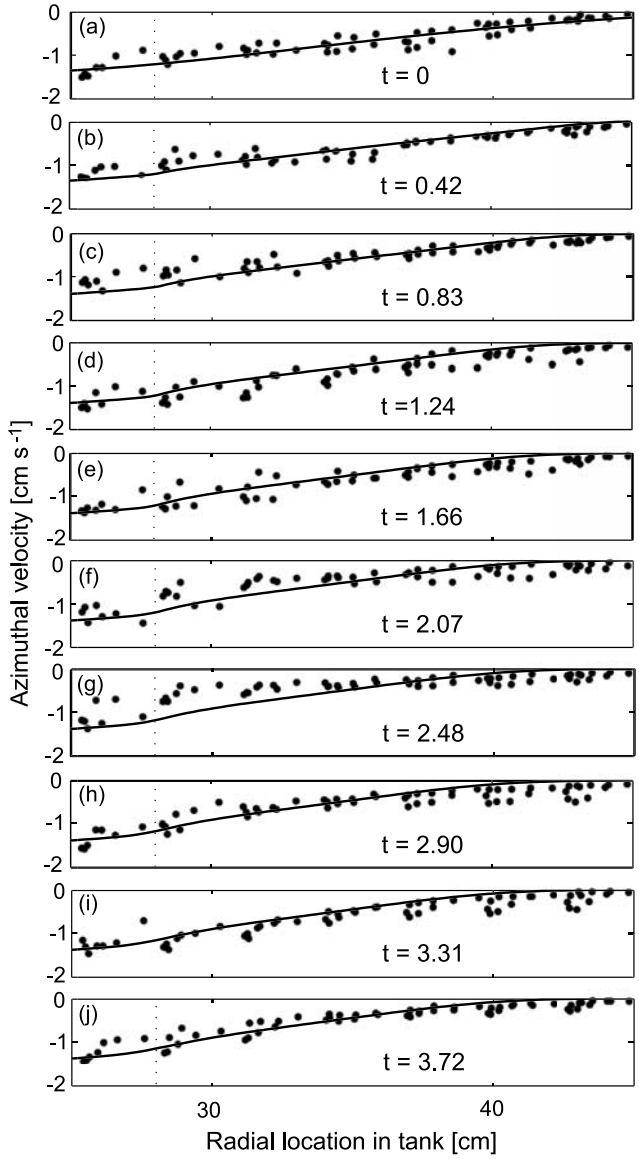

Figure 7. Same as Figure 6, but for a stratified fluid (trial 1, $N = 2.2\ s^{-1}$, $f = 0.52\ s^{-1}$).

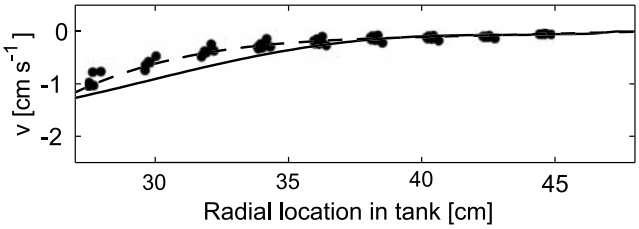

Figure 8. Comparison of numerical prediction of spin-up without a canyon (solid line) to laboratory spin-up with a canyon (dashed line, fit to dots). The difference between the two lines (Δv) can be used to find the impulse $F\Delta t$ imposed on the fluid by the canyon.

where v_{up} is the average cross–shelf break velocity induced by the canyon, and $V \approx W_{sb}L^2(f/N)Ro^{2/3}$ is the volume of affected water within the canyon, where W_{sb} is the width of the canyon at the shelf break (Figure 4). Multiplying v_{up} by the cross-sectional area of the canyon mouth (proportional to V/L) gives the upwelling flux through the canyon onto the shelf as

$$\Phi = C_d L N^{-1} Ro^{2/3} U^2. \quad (15)$$

[45] Our laboratory experiments can be used to calibrate this flux model for the strength of upwelling, provided that shelf break velocity, stratification, and Coriolis frequency are known. The laboratory canyon is a simplified version of Astoria Canyon, and the laboratory model is designed to have similar Ekman, Rossby, Froude, and Burger numbers to Astoria Canyon (Table 1). If we assume from continuity that $w_{up} = v_{up}HL^{-1}$, then for $U = 10^{-1}$ m s^{-1}, $N = 10^{-2}$ s^{-1}, $f = 10^{-4}$ s^{-1}, $L = 2.2 \times 10^4$ m, and $H = 150$ m, the mean upwelling velocity over Astoria Canyon is $w_{up} \approx 2 \times 10^{-5}$ m s^{-1}, a value that agrees with numerical predictions [e.g., *Klinck*, 1996] averaged over the top of the entire canyon. This value, however, is about an order of magnitude lower than maximum upwelling rates observed at the head of Astoria Canyon [*Hickey*, 1997]. This difference is due to our method of length scales to determine currents from our predicted flux; no other geometrical or physical attributes are considered. Using the observations of $w_{up} = 50$ m d^{-1} for upwelling at the head of Astoria Canyon made by *Hickey* [1997] (under slightly stronger along-shelf currents) to determine flux (velocity × width × length) would give an unreasonable flux of 0.2 Sv. To put this number in context, consider that a quick scaling (along-shelf velocity of 0.1 m s^{-1}, depth of 100 m, and width of

Table 3. Values Used for Testing Drag Parameterization in Figure 9[a]

f, s^{-1}	N, s^{-1}	U, 10^{-2} m s^{-1}	δU, 10^{-2} m s^{-1}	Ro	S_c	F_d, 10^{-5} N	δF_d, 10^{-5} N
0.52	2.2	1.38	0.03	0.66	1.06	9.67	1.82
0.52	2.2	1.17	0.03	0.56	1.06	7.36	1.22
0.52	2.2	1.04	0.02	0.50	1.06	5.51	1.08
0.52	2.2	0.89	0.03	0.43	1.06	4.55	1.32
0.52	2.2	0.76	0.05	0.37	1.06	2.48	1.56
0.52	2.2	0.73	0.03	0.35	1.06	2.63	1.26
0.52	2.2	0.60	0.06	0.29	1.06	1.74	1.65
0.52	2.2	0.58	0.06	0.28	1.06	2.10	1.57
0.52	2.2	0.57	0.03	0.27	1.06	0.66	1.02
0.52	2.2	0.55	0.08	0.26	1.06	2.49	1.88
0.52	2.2	0.45	0.07	0.22	1.06	1.38	1.79
0.52	4.4	1.71	0.05	0.82	2.12	9.02	2.68
0.52	4.4	1.69	0.05	0.81	2.12	8.26	1.94
0.52	4.4	1.68	0.05	0.81	2.12	8.75	2.75
0.52	4.4	1.62	0.06	0.78	2.12	5.47	2.23
0.52	4.4	1.19	0.04	0.57	2.12	3.66	1.83
0.52	4.4	1.13	0.04	0.54	2.12	3.15	1.50
0.70	2.2	1.68	0.06	0.60	0.79	16.32	3.65
0.70	2.2	1.47	0.04	0.53	0.79	12.10	2.38
0.70	2.2	1.27	0.03	0.45	0.79	7.00	2.09
0.70	2.2	1.22	0.02	0.44	0.79	8.88	1.91
0.40	2.2	1.49	0.03	0.93	1.38	12.27	1.12
0.40	2.2	1.42	0.02	0.89	1.38	10.17	1.05
0.40	2.2	1.32	0.02	0.83	1.38	7.35	1.00
0.40	2.2	1.17	0.03	0.73	1.38	2.26	1.18

[a]The uncertainties in shelf break velocity, δU, and drag force, δF_d, are used to generate the uncertainties shown in Figure 9.

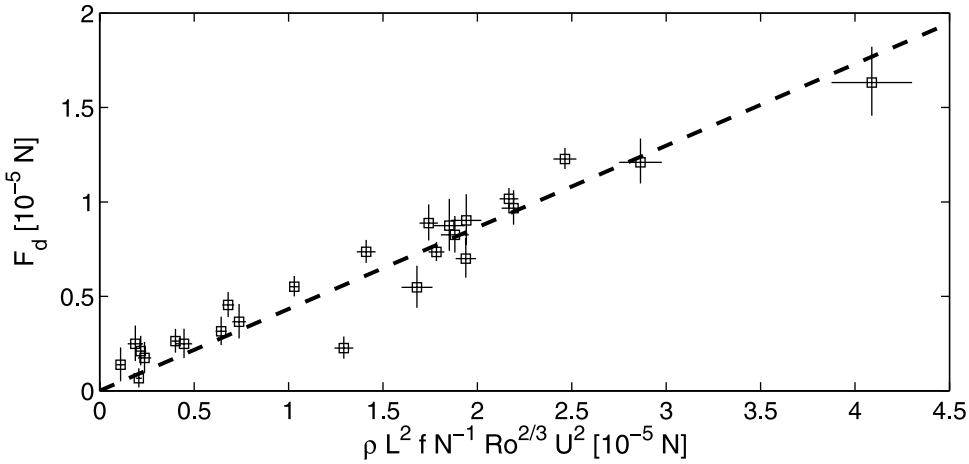

Figure 9. Results of all experiments showing the relationship between the drag force, F_d, and $\rho L^2 F N^{-1} Ro^{2/3} U^2$. The regression for a line of best fit is shown. Its slope is the drag coefficient, $C_d = 0.43 \pm 0.02$. The vertical error bars represent the error in F_d propagated from velocities entered as initial conditions into the heuristic model. The horizontal error bars arise from the propagation of uncertainty in U.

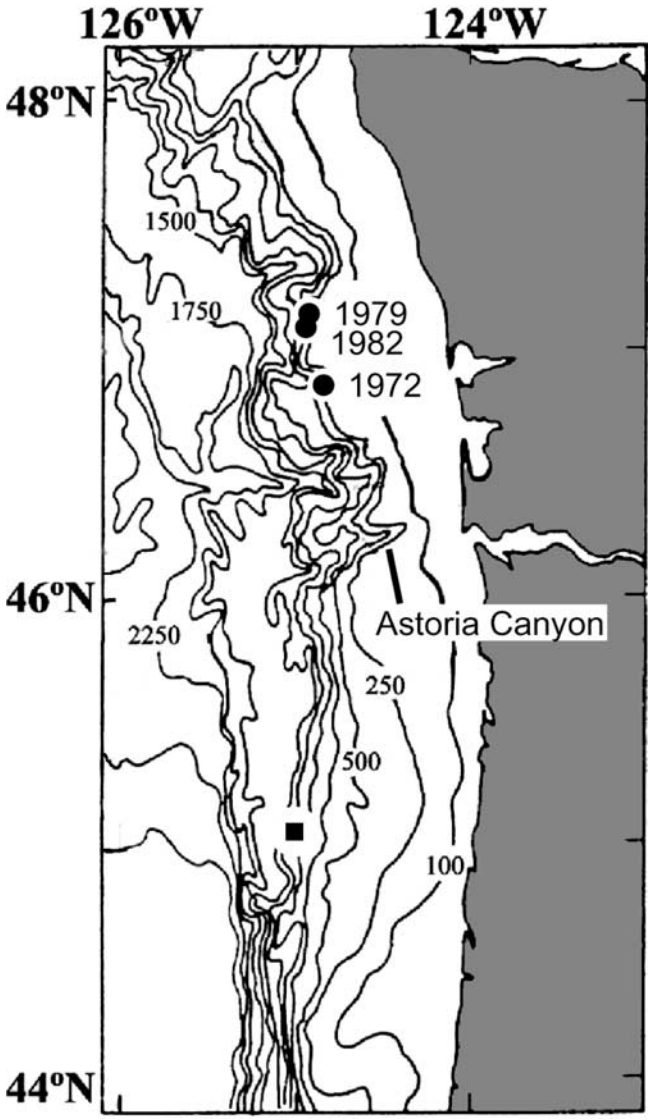

Figure 10. Bathymetry near Astoria Canyon. Locations of current meters in 1972, 1979, and 1982 are plotted as solid circles north of the canyon. The location used for wind data is shown as a solid square south of the canyon. Figure after *Hickey* [1995].

50 km) suggests the along-shelf transport over the Washington shelf is only about 0.5 Sv. The reason for the discrepancy between modelled and observed values for w_{up} is that the upwelling strength over the canyon is not homogeneous. There is strong upwelling at the head of the canyon, but it is not sustained over the entire canyon [*Klinck*, 1996].

[46] To predict a time series of upwelling through Astoria Canyon, we obtained current meter measurements (described by *Hickey* [1989]) at near–shelf break depths approximately 100 km north of Astoria (Figure 10). This site is along a relatively uncorregated segment of the shelf break, however, and currents in the Oregon-Washington region are well correlated over 500 km distances [*Huyer et al.*, 1975]. It is upstream of Astoria during upwelling-favorable conditions, hence Astoria should not affect the flow past the current meters.

[47] For comparison, NCEP-NCAR reanalysis wind data [*Kistler et al.*, 2001] are used to approximate wind-induced upwelling over the same periods that current meter data are available. The data, provided by the NOAA-CIRES Climate Diagnostic Center, Boulder, Colorado, were acquired from their Web site http://www.csc.noaa.gov. The nearest grid point in the data set is 100 km south of Astoria, but the dominant wind scales for the region exceed 500 km [*Halliwell and Allen*, 1987]. If an Ekman balance is assumed, then by continuity the wind-induced upwelling flux onto the shelf over Astoria Canyon is

$$\Phi_w = -W_{sb}\tau\rho^{-1}f^{-1}, \tag{16}$$

where $W_{sb} = 1.6 \times 10^4$ m is the width of Astoria Canyon at the shelf break, and τ is the wind stress parallel to the shelf break and is calculated from wind speed following *Smith* [1988]. Note that sign of this flux does not represent the water that is advected off the shelf by wind forcing, but rather that which is required to balance it.

[48] Current meter data were collected in 1972, 1979, and 1982, and are described by *Hickey* [1989]. Currents gathered in 1982 cover a nine day period, and the 1979 data cover the entire summer season. In 1972, current meters recorded water velocities from 21 July to 19 September but did not capture southward currents over the shelf necessary to produce upwelling through Astoria Canyon. These data were used to support the 1979 data, however, and are discussed below.

[49] Current meters from 1982 provide data from 14 to 22 June at a depth of 146 m. These currents were collected just past the shelf edge in 235-m-deep water. During the time the data were collected, southward along–shelf break currents reached values close to 0.06 m s^{-1}, resulting in a moderate upwelling event in Astoria canyon (Figure 11). Upwelling-favorable winds blew consistently over the entire sampling period. Currents near the shelf break and the average wind-induced transport over the period are also shown. The currents show a periodic fluctuation, likely due to tides, but the upwelling event is still clear. These measurements were made during a period of moderate wind forcing, with along–shelf break winds blowing steadily at about 3.5 m s^{-1}.

[50] To examine seasonal trends, we turn to the 1979 data set, where currents were measured at 152 m in 160 m of water. Currents collected from a mooring at a similar location in 1972, however, provided data at 110 m and 160 m depth in water that was 175 m deep. The currents from 160 m were able to predict the 110 m currents successfully (see Appendix A for details). The 1972 data suggest almost no rotation or change in velocity. Hence for synoptic trends of canyon upwelling, the 1979 data should be adequate despite their proximity to the bottom. We use them without compensating for their depth to produce a time series of upwelling through Astoria Canyon (Figure 12). This figure also shows estimated on-shelf flux of deep water from wind forcing based on (16) for comparison. Over an entire summer season, the integrated flux through the canyon is less than that imposed by winds, but of similar order. During a strong upwelling event, such as that seen in mid-May, the upwelling flux through Astoria is an order of magnitude larger than that imposed by wind-

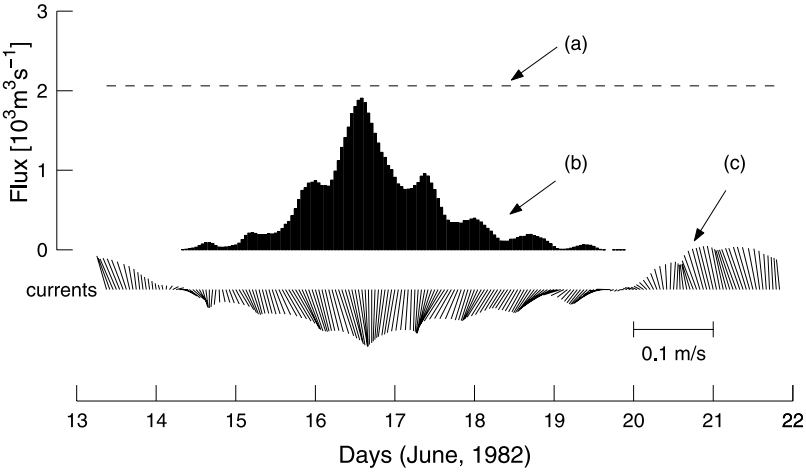

Figure 11. Predicted flux through Astoria Canyon in mid-June 1982 during a moderate upwelling event. (a) Dashed line shows mean wind-driven upwelling flux above Astoria Canyon over the time period. (b) Predicted on-shelf flux of water through Astoria Canyon using (15). (c) Current meter velocity measurements used in (15). For the stick plot the frame is rotated to coordinates aligned with the local bathymetry (downward corresponds to the upwelling-favorable, along-shelf direction).

induced upwelling over a similar width of shelf break. This peak in upwelling is associated with along-shelf currents of nearly 0.15 m s^{-1}.

[51] The estimates from our laboratory may underpredict real values in the ocean. In fitting the drag parameterization (13), we used surface values of the shelf break velocity. Numerical models of flow in the laboratory [*Allen et al.*, 2003] suggest that the interior flow just above the boundary layer on the shelf may be traveling up to 20% slower than the surface flow. Since $F_p \propto C_d U^{8/3}$ (note that $U^{2/3}$ is included from the Rossby number), the drag coefficient C_d, and therefore the flux Φ, may be too small by a factor of two.

[52] Our predictions for the depth below the canyon rim from which water is upwelled, $H_c \propto Ro^{2/3} LfN^{-1}$, likely has a proportionality coefficient of less than one. Integrating the Bernoulli function along a streamline suggests that if water from H_c is to clear the canyon rim, the vertical Froude number $Fr_v = U/(NH_c) \geq 1$ [e.g., *Snyder*, 1985]. Satisfying this condition implies a proportionality coefficient of 0.6 for our experiments. This coefficient is included in C_d here and will not affect values of Φ. However, it is of importance if the source depth of water upwelled through the canyon is of interest (for example, if nutrient dynamics are a concern).

[53] Even in a simple laboratory model, flow through a submarine canyon is complex. While this work gives a good approximation for the seasonal cross–shelf break mass flux due to upwelling in Astoria canyon, it also shows the many limitations of our current state of knowledge about these

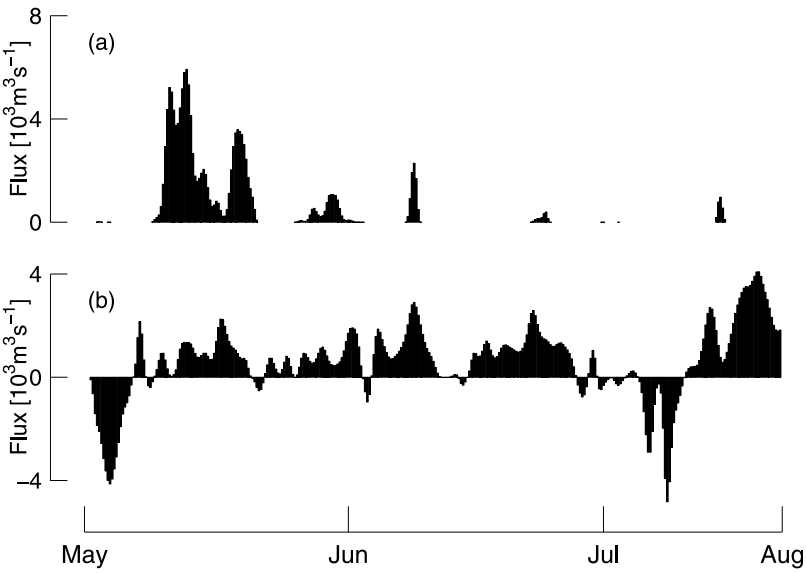

Figure 12. Comparison of flux prediction through Astoria Canyon to wind-forced upwelling over the canyon during the summer months of 1979. (a) Predicted on-shelf flux of water through Astoria Canyon using equation (15). (b) Wind-induced on-shelf flux over Astoria Canyon.

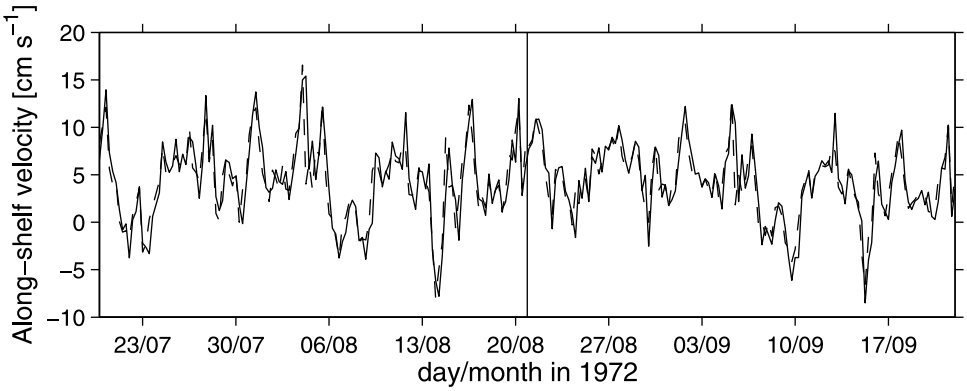

Figure A1. Comparison of along-shore currents at 110 m depth (solid line) to currents predicted with the 160 m data set (dashed line). The vertical line at 21 August 1972 indicates the division of the data sets into the training and validation parts. The constants α and β in (A1) were determined without considering currents collected after this date.

processes. Greater analysis of the nonlinear flow field within a submarine canyon needs to be performed.

6. Conclusions

[54] It has long been believed that canyons have a considerable influence on shelf break upwelling. We use our laboratory results with a season-long time series of oceanographic data to show that a first-order effect over an extended period of time may exist. This longer-scale impact on shelf-slope exchange flow, suggests a "climatic effect" of Astoria Canyon rather than an isolated "weather effect." Such effects may have considerable implications for describing spatial variability in shelf-slope exchange, something that is often homogenized in global ocean models.

[55] Previously, upwelling through submarine canyons has been studied under strong upwelling conditions, where geostrophic along shelf currents are as large as 20 cm s^{-1}. As we predict that the upwelling flux is related to $U^{8/3}$, these strong events will give the largest individual contributions. Such events are relatively uncommon, however. None occurred in the 1979 data set we present. This leads us to believe that the long-term contribution of the strongest events will be relatively low.

[56] Astoria is an isolated canyon, and so its seasonal contribution to upwelling along the Washington shelf break will be limited. It has recently been demonstrated that closely spaced canyons have a strong regulating effect on the shelf break upwelling field [*Sobarzo and Djurfeldt*, 2004]. There are many sections of shelf break (such as those off southern British Columbia and Alaska) that are cut by numerous canyons. Their collective effect on regional upwelling is likely to be of greater importance than what we determined for Astoria Canyon. In order to expand our results to other canyons, the effects of different canyon geometries must be considered in greater detail.

Appendix A: Near-Bottom Current Meter Data

[57] Current meter data in 1979 were collected from 2 May to 5 August. They were collected at a depth of 152 m, only 8 m above the bottom. This left uncertainty as to whether the data were too deep in the boundary layer to be used.

[58] To examine the relationship between the current meters at 160 m and 110 m depth in 1972, the current meter data were represented as time series of the complex scalar, $w'_k(t_m) = u'_k(t_m) + iv'_k(t_m)$, where u' and v' are two orthogonal horizontal velocity components onto which the currents are projected, the subscript $k = 1, 2$ represents the lower and upper current meters, respectively, and the subscript m represents the discretized time step in the time series. We want to test how well w_1 predicts w_2 using the simple linear relationship

$$\hat{w}_2(t) = \alpha + \beta w'_1(t) + \varepsilon(t), \tag{A1}$$

where α, β, and ε are complex.

[59] The mean, $\bar{w}_k$, is removed, leaving $\tilde{w}_k$, and $\alpha \equiv \bar{w}_2 - \beta\bar{w}_1$. Our estimate for β is $\hat{\beta}$ and is solved with the complex regression

$$\hat{\beta} = \frac{\sum_{m=1}^{M} \tilde{w}_1(t_m)^* \tilde{w}_2(t_m)}{\sum_{m=1}^{M} \tilde{w}_1(t_m)^* \tilde{w}_1(t_m)}, \tag{A2}$$

where the asterisk represents the complex conjugate. ε is the error in the model and is $\varepsilon = w'_2 - \alpha - \hat{\beta}\tilde{w}_1$.

[60] The 1972 data set contains 258 points. As we wish to predict data on an independent time series, we divide $w'_k(t)$ into two equal parts. The first half is used for the regression ($M = 129$), and the second half is used to validate the method.

[61] The skill of the model is tested on $\tilde{w}_k^2$ by comparing the variance in ε to the variance in $\tilde{w}_2^2$:

$$\gamma^2 = \frac{\mathrm{var}(\varepsilon)}{\mathrm{var}(\tilde{w}_2^2)}. \tag{A3}$$

The results show good agreement over the training and validation sections of the data set (Figure A1). The training section of the data provide $\hat{\beta} = 0.89 + 0.09i$. Over the validation domain, $\gamma^2 = 0.23$. If (A3) were determined for the training domain, then its value would be equivalent to

$1 - R^2$. The value for $\hat{\beta}$, indicates that from w_1 to w_2, the variance decreases and rotates by about 7%. The change in mean velocity vector between the two current meters is less than 1%, with a rotation of less than 0.5 degrees ($\bar{w}_2/\bar{w}_1 = 0.999 + 0.007i$). Hence for the synoptic purposes here, extrapolating the currents near the bottom to be similar to those higher in the water column is reasonable.

[62] **Acknowledgments.** The authors gratefully acknowledge the insight and assistance of Rich Pawlowicz and Noboru Yonemitsu for developments of theory and laboratory methods, respectively. Comments from Dan Kelley as well as two anonymous reviewers improved the manuscript considerably. Current meter data, which allowed us to apply our results in an oceanic environment, were kindly provided by Barbara Hickey. The assistance provided by Amy Waterhouse was instrumental in producing Figure 2. This work was supported by an NSERC strategic grant to S. Allen.

References

Allen, S. E. (1996), Topographically generated, subinertial flows within a finite length canyon, *J. Phys. Oceanogr.*, *26*, 1608–1632.

Allen, S. E. (2000), On subinertial flow in submarine canyons: Effect of geometry, *J. Geophys. Res.*, *105*, 1285–1297.

Allen, S. E., C. Vindeirinho, R. E. Thomson, M. G. Foreman, and D. L. Mackas (2001), Physical and biological processes over a submarine canyon during an upwelling event, *Can. J. Fish. Aquat. Sci.*, *58*, 671–684.

Allen, S. E., M. S. Dinniman, J. M. Klinck, D. D. Gorby, A. J. Hewett, and B. M. Hickey (2003), On vertical advection truncation errors in terrain-following numerical models: Comparison to a laboratory model for upwelling over submarine canyons, *J. Geophys. Res.*, *108*(C1), 3003, doi:10.1029/2001JC000978.

Batchelor, G. K. (1967), *An Introduction to Fluid Dynamics*, 615 pp., Cambridge Univ. Press, New York.

Benton, E. R., and A. Clark (1974), Spin-up, *Ann. Rev. Fluid Mech.*, *6*, 257–280.

Boyer, D. L., D. B. Haidvogel, and N. Pérenne (2004), Laboratory-numerical model comparisons of canyon flows: A parameter study, *J. Phys. Oceanogr.*, *34*, 1588–1609.

Durrieau de Madron, X. (1994), Hydrography and nepheloid structure in the Grand-Rhone canyon, *Cont. Shelf Res.*, *14*, 457–477.

Freeland, H., and K. Denman (1982), A topographically controlled upwelling center off Vancouver Island, *J. Mar. Res.*, *40*, 1069–1093.

Greenspan, H. (1968), *The Theory of Rotating Flows*, Cambridge Univ. Press, New York.

Greenspan, H., and L. Howard (1963), On a time-dependent motion of a rotating fluid, *J. Fluid Mech.*, *17*, 385–404.

Halliwell, G. H., Jr., and J. S. Allen (1987), Large-scale coastal wind field along the west coast of North America, 1981–1982, *J. Geophys. Res.*, *92*, 1861–1884.

Hart, J. (2000), A note on the nonlinear corrections to the Ekman layer pumping velocity, *Phys. Fluids*, *12*, 131–135.

Hickey, B. M. (1989), Patterns and processes of circulation over the Washington continental shelf and slope, in *Coastal Oceanography of Washington and Oregon*, edited by M. Landry and B. Hickey, pp. 41–115, Elsevier, New York.

Hickey, B. M. (1995), Coastal submarine canyons, in *Aha Hulikoa: Topographic Effects in the Ocean*, edited by P. Muller and D. Henderson, pp. 95–110, Sch. of Ocean and Earth Sci. and Technol., Honolulu, Hawaii.

Hickey, B. M. (1997), The response of a narrow canyon to strong wind forcing, *J. Phys. Oceanogr.*, *27*, 697–726.

Hogg, N. G. (1973), On the stratified Taylor column, *J. Fluid Mech.*, *58*, 517–537.

Holton, J. R. (1965), The influence of viscous boundary layers on transient motions in a stratified fluid: part I, *J. Atmos. Sci.*, *22*, 402–411.

Huyer, A., B. M. Hickey, J. D. Smith, R. L. Smith, and R. D. Pillsbury (1975), Alongshore coherence at low frequencies in currents observed over the continental shelf off Oregon and Washington, *J. Geophys. Res.*, *80*, 3495–3505.

Kinsella, E. D., A. E. Hay, and W. W. Denner (1987), Wind and topographic effects on the Labrador current at Carson canyon, *J. Geophys. Res.*, *92*, 10,853–10,869.

Kistler, R., et al. (2001), The NCEP-NCAR 50-year reanalysis: Monthly means CD-ROM and documentation, *Bull. Am. Meteorol. Soc.*, *82*, 247–267.

Klinck, J. (1996), Circulation near submarine canyons: A modelling study, *J. Geophys. Res.*, *101*, 1211–1223.

MacCready, P., and P. B. Rhines (1991), Buoyant inhibition of Ekman transport on a slope and its effect on stratified spin-up, *J. Fluid Mech.*, *223*, 631–661.

Oster, G. (1965), Density gradients, *Sci. Am.*, *213*, 70–76.

Pedlosky, J. (1987), *Geophysical Fluid Dynamics*, 710 pp., Springer, New York.

Pérenne, N., J. Verron, D. Renouard, D. L. Boyer, and X. Zhang (1997), Rectified barotropic flow over a submarine canyon, *J. Phys. Oceanogr.*, *27*, 1868–1893.

Pérenne, N., D. B. Haidvogel, and D. L. Boyer (2001a), Laboratory-numeric model comparisons of flow over a coastal canyon, *J. Atmos. Oceanic Technol.*, *18*, 235–255.

Pérenne, N., J. W. Lavelle, D. C. Smith IV, and D. L. Boyer (2001b), Impulsively started flow in a submarine canyon: Comparison of results from laboratory and numerical results, *J. Atmos. Oceanic Technol.*, *18*, 1698–1718.

Press, W., B. Flannery, S. Teukolsky, and W. Vetterling (1986), *Numerical Recipes: The Art of Scientific Computing*, 818 pp., Cambridge Univ. Press, New York.

Raffel, M., C. Willert, and J. Kompenhaus (1998), *Particle Image Velocimetry: A Practical Guide*, Springer, New York.

She, J., and J. M. Klinck (2000), Flow near submarine canyons driven by constant winds, *J. Geophys. Res.*, *105*, 28,671–28,694. (Correction, *J. Geophys. Res.*, *106*, 2689, 2001.)

Signorini, S. R., A. Münchow, and D. Haidvogel (1997), Flow dynamics of a wide Arctic canyon, *J. Geophys. Res.*, *102*, 18,661–18,680.

Smith, S. D. (1988), Coefficients for sea surface wind stress, heat flux, and wind profiles as a function of wind speed and temperature, *J. Geophys. Res.*, *93*, 15,467–15,472.

Snyder, W. H. (1985), Fluid modeling of pollutant transport and diffusion in stably stratified flows over complex terrain, *Ann. Rev. Fluid Mech.*, *17*, 239–266.

Sobarzo, M., and L. Djurfeldt (2004), Coastal upwelling process on a continental shelf limited by submarine canyons, Concepción, central Chile, *J. Geophys. Res.*, *109*, C12012, doi:10.1029/2004JC002350.

Sveen, J. (2000), *An Introduction to MatPIV v.1.4*, report, 18 pp., Univ. of Oslo, Norway.

S. E. Allen, Department of Earth and Ocean Sciences, University of British Columbia, Vancouver, British Columbia, Canada V6T 1Z4. (sallen@eos.ubc.ca)

R. Mirshak, Department of Oceanography, Dalhousie University, Halifax, Nova Scotia, Canada B3H 2H9. (ramzi.mirshak@phys.ocean.dal.ca)